Geochemical Journal, Vol. 39, pp. 213 to 226, 2005

# Geochemistry of the Mirador Formation (Late Eocene-Early Oligocene), southwestern Venezuela: Chemostratigraphic constraints on provenance and the influence of the sea level

KATYA REÁTEGUI,[1] MANUEL MARTÍNEZ,[1]* IVÁN ESTEVES,[2] JOSÉ V. GUTIÉRREZ,[3] ALEJANDRO MARTÍNEZ,[1] WILLIAMS MELÉNDEZ[1] and FRANCO URBANI[4]

[1]Centro de Geoquímica, Instituto de Ciencias de la Tierra, Facultad de Ciencias, Universidad Central de Venezuela, Apartado Postal 3895, Caracas 1010A, Venezuela
[2]Instituto Zuliano de Investigación Tecnológica INZIT-CICASI, Carretera La Cañada, Km 14, Maracaibo, Venezuela
[3]Centro de Geología, Instituto de Ciencias de la Tierra, Facultad de Ciencias, Universidad Central de Venezuela, Apartado Postal 3895, Caracas 1010 A, Venezuela
[4]Escuela de Geología, Minas y Geofísica, Facultad de Ingeniería, UCV, Apto 1053, Caracas 1010 A, Venezuela

(*Received May 17, 2004; Accepted November 9, 2004*)

A geochemical study was carried out on Eocene-Lower Oligocene sedimentary rocks (the Mirador Formation) from the southern Lake Maracaibo Basin, western Venezuela. The goal of this work was the identification of source rock composition and tectonic settings of source areas, and their temporal changes. The geochemistry was also used to investigate attributes of the paleoenvironment. Eighty-nine rock samples were collected and the bulk inorganic geochemistry ($Al_2O_3$, $SiO_2$, $TiO_2$, $Fe_2O_3$, MnO, CaO, MgO, $K_2O$, Li, B, Sc, V, Cr, Ni, Zn, Rb, Y, Mo, La, Ce and Th) was determined by ICP-AES; total sulfur was determined in a LECO SC-432 analyzer. Multivariate statistical tools were employed to evaluate the correlation between the different variables. Through cluster-constrained analysis, four subdivisions, or main chemofacies, were defined and correlated with the significant lithologic units. The tectonic setting for the source rock could be a passive margin, and a mixed source was inferred, consisting of recycled sedimentary rocks and igneous and/or meta-igneous rocks of predominantly felsic composition. The most marine-influenced lithological units occur at the bottom of the section.

Keywords: chemostratigraphy, provenance, geochemistry, Venezuela, paleoenvironments

## INTRODUCTION

A major goal in sedimentary studies is to find useful tools to determine environmental conditions and the provenance of sediments. The geochemistry of sedimentary rocks delineates the provenance and provides clues to the plate tectonic evolution. The geochemical signature of detrital sediments is primarily controlled by the composition of the source rocks, and to a minor extent, by weathering and diagenetic processes (Asiedu *et al*., 2000; Totten *et al*., 2000). Therefore, geochemical tracers can be used to identify source rocks and weathering processes (Cullers *et al*., 1988; Nesbitt, 1979). When geochemical data are evaluated in the context of the stratigraphic log, a chemostratigraphic study is accomplished, involving the application of major and trace element geochemistry for the characterization of the sedimentary sequence into geochemically distinct units (Winchester and Max, 1996; Das, 1997; Jarvis *et al*., 1998; Pearce *et al*., 1999). Chemostratigraphy can be carried out with isotopic data (Brasier and Shields, 2000; Ehrenberg *et al*., 2000) or by combining several chemical indices (Crespo *et al*., 1999; Reyment and Hirano, 1999; Reinhardt and Ricken, 2000; Stevenson *et al*., 2000). Other aspects revealed by chemostratigraphic studies are paleoproductivity, climatic changes and chemical cyclicity in processes involving basin sedimentation (Bellanca *et al*., 1996; Villamil, 1996; Dayong *et al*., 1999).

The Mirador Formation (Eocene-Early Oligocene) is a suitable sedimentary sequence for a chemostratigraphic study because of its barren condition, wide geographical extent, and its position in the hydrocarbon-bearing sequence of the Lake Maracaibo Basin. The aim of this study is to reconstruct paleoenvironmental conditions in the Mirador Formation by using bulk geochemical data from whole rock analyses. These analyses provide information about the provenance of the sediments relating to sediment supply, weathering style, redox conditions and the

*Corresponding author (e-mail: manmarti@gea.ciens.ucv.ve)

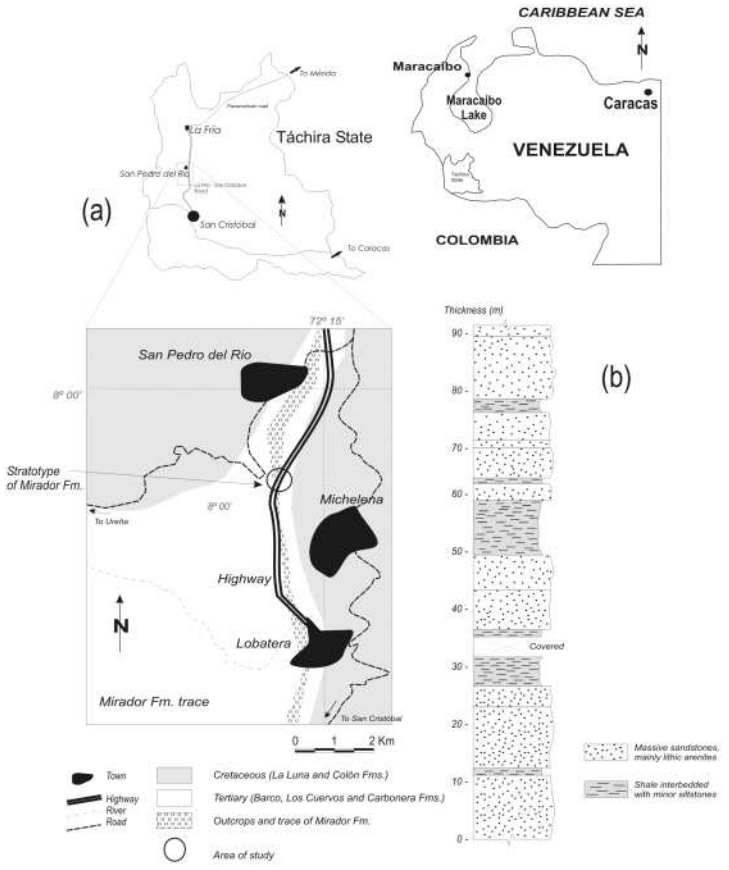


*Fig. 1. Sketch map (a) showing the trace of Mirador sandstones at the Lobatera-Colón area, Táchira State, and the sampling location (stratotype of Mirador Fm). (b): Simplified stratigraphic column of the Mirador Formation in the studied area.*

influence of sea level. Although there are some prior geologic, petrographic and sedimentologic studies of the Mirador Formation, only a few have attempted to study the bulk geochemistry of this unit. This study focuses on the geochemical features of the strata and their vertical variations (Chemostratigraphy) for defining chemical facies (chemofacies) and relating these to changes in provenance and paleoenvironmental conditions.

## GEOLOGICAL SETTING

The southernmost Lake Maracaibo Basin comprises a thick sedimentary cover overlying a Precambrian and Paleozoic igneous-metamorphic complex, in a tectonic framework dominated, during the Cretaceous, by a passive margin, probably the southern margin of the Tethyan Ocean (Parnaud *et al*., 1995). This framework gradually shifted to a foreland basin during the Paleogene.

At the beginning of the Cretaceous a marine transgression caused inundation of the Guyana shield. This transgression is correlated to the eustatic changes that occurred worldwide and lasted until the Cenomanian-Campanian (Parnaud *et al*., 1995). Regression started at the beginning of the Late Cretaceous. Simultaneously, toward the west, the Pacific volcanic arc collision formed a foreland basin. During the Late Paleocene-Middle Eocene, emplacement of the "Lara Nappes" began to the northern end of the Lake Maracaibo basin. These nappes gradually encroached eastward, forming new foreland basins. This flexural deformation is reflected in a suite of transgressive and regressive cycles of Eocene age.

The sedimentary sequence of the southern Lake Maracaibo Basin begins with the red-bed, Jurassic La Quinta Formation, which disconformably overlies the basement (González de Juana *et al*., 1980). The Cretaceous sedimentation is represented by the Rio Negro Formation (basal conglomerates), the Cogollo Group, and La Luna, Colón and Mito Juan Formations. The maximum of the Cretaceous transgression is marked by the La Luna Formation, considered the main hydrocarbon source rock for the Lake Maracaibo Basin; the subsequent gradual regression, which continues through the Paleogene, is

demarcated by the Colón and Mito Juan Formations.

The Paleogene regression is marked by a gradual shift in sedimentary environments, from open-sea, littoral and delta plain, towards estuarine-fluvial systems (Orocué Group and the Mirador Formation). In the Táchira area, sediments derived from the shallow shelf to littoral zones and tidal flats are represented by massive and laminated sandstones, rich in flaser lamination, and siltstones from the Barco Formation, of the Orocué Group. Overlying the Barco Formation is the Los Cuervos Formation, which is characterized by siltstones, shales, some sandstone and coal beds assigned to a lower to upper delta plain. The Mirador Formation overlies the Los Cuervos Formation.

Located in the southern Lake Maracaibo Basin, Venezuela, the Mirador Formation outcrops in the southeastern Perijá Mountains, the western flank of the Andean Cordillera and adjacent areas in Colombia. The Mirador Formation is composed of thick, massive sandstones, interbedded with scarce shales and siltstones, with a total thickness varying from 80 to 550 m (Fig. 1). Sandstones are mainly quartz-arenite and sub-lithic arenite. This unit was deposited in a fluvial-estuarine environment (Paparoni, 1993) and can be correlated to the Misoa Formation of the northern Lake Maracaibo Basin, the main reservoir rock of the petroleum system of this basin (González de Juana *et al*., 1980).

Palynologic studies (Colmenares and Teran, 1990) show that the Mirador Formation was deposited during the Eocene to Early Oligocene; a hiatus is reported, corresponding to the Late Eocene (Brondjick, 1967). The upper contact of the Mirador Formation is concordant with the Carbonera Formation.

## Samples and Methodology

*Sampling*

Eighty-nine samples of sandstones, siltstones and shales, taken on average at 1-m stratigraphic intervals, were collected from the Mirador Formation along a road cut on the San Cristobal-La Fria highway, near the town of San Pedro del Rio (Fig. 1-a). An excellent and complete exposure of the sedimentary succession is present here. The site is considered the type section in Venezuela (the Mirador Formation was first defined in Colombia). Sandstone beds at the sampling site are well-stratified, massive, with variable thickness, and are interbedded with thin shales. Analysis of the sequence allows defining at least 5 lithological associations or "strata packages": Three sandy associations (lithological $S_1$, $S_2$ and $S_3$) separated by two shale facies (named $Sh_1$ and $Sh_2$) clearly dividing the section (Fig. 1-b). The bottoms of sandstone beds overlying the thick shales show cut and fill structures, with angular relationships, providing evidence of erosional surfaces.

*Petrography*

Thin sections were prepared in the standard manner, in selected sandstones from distinctive points of the stratigraphic section. Optically identifiable components in the sandstones are mono-and poly-crystalline quartz, chert and muscovite. No orthoclase grains were observed. Accessory minerals identified are glauconite, epidote and staurolite. Sandstones studied were classified as sublitharenite/lithic arenite, and quartz/lithic wacke, making use of the Pettijohn triangle. Predominant contacts between grains were longitudinal and concave-convex, suggesting a moderate stage of diagenesis.

*Analytical procedures*

Samples were ground in a tungsten carbide ball-mill. Dissolution of samples was made by sinterizing with sodium peroxide, as described by Borsier (1991). It entails: about 0.30 g of rock powder was weighed, and sodium peroxide was added to yield a peroxide to rock ratio of 3:1, the mixture was placed in a zirconium crucible as alternate layers of peroxide and sample. The crucible was heated to 450°C for 1 hour; then the sinterized material was dissolved in dilute HCl. Geochemical data were obtained using a Jobin Yvon, model JY 24 ICP-AES. In this study, eight major elements, expressed as % w/w oxides ($Al_2O_3$, $SiO_2$, $TiO_2$, $Fe_2O_3$, MnO, CaO, MgO and $K_2O$) and thirteen trace elements, expressed as $\mu$g/g (Li, B, Sc, V, Cr, Ni, Zn, Rb, Y, Mo, La, Ce and Th) were determined by this technique. Total sulfur was determined in a LECO SC-432 analyzer. Total Organic Carbon (TOC) was determined in a coulometric carbon analyzer (Coulometrics). Data quality was assessed by the dissolution and analysis of well-characterized international (granite USGS-G2 and andesite USGS AGV-1) and in-house rock reference materials.

*Statistical considerations*

The properties of the data need to be reviewed as a preliminary step to discussing appropriate methods of statistical analysis. First, the data are highly multivariate; there being 22 variables in a sample size of N = 89. Second, most standard methods of multivariate analysis are not generally applicable to geochemical data without some appropriate transformation. Previous exploratory data analysis and descriptive statistics using Dixon and Kronmal (1965) criteria for class interval choice indicate a lognormal distribution for trace element compositions. For this reason, all matrix data were transformed to the respective natural logarithmic values, for a better approach to a normal distribution; this adjustment does not modify the original distribution, but allows the use of parametric statistics. All transformed data were then standardized, for an arithmetic mean = 0 and a standard deviation = 1, applying the formula (Reiman and Filmoser,

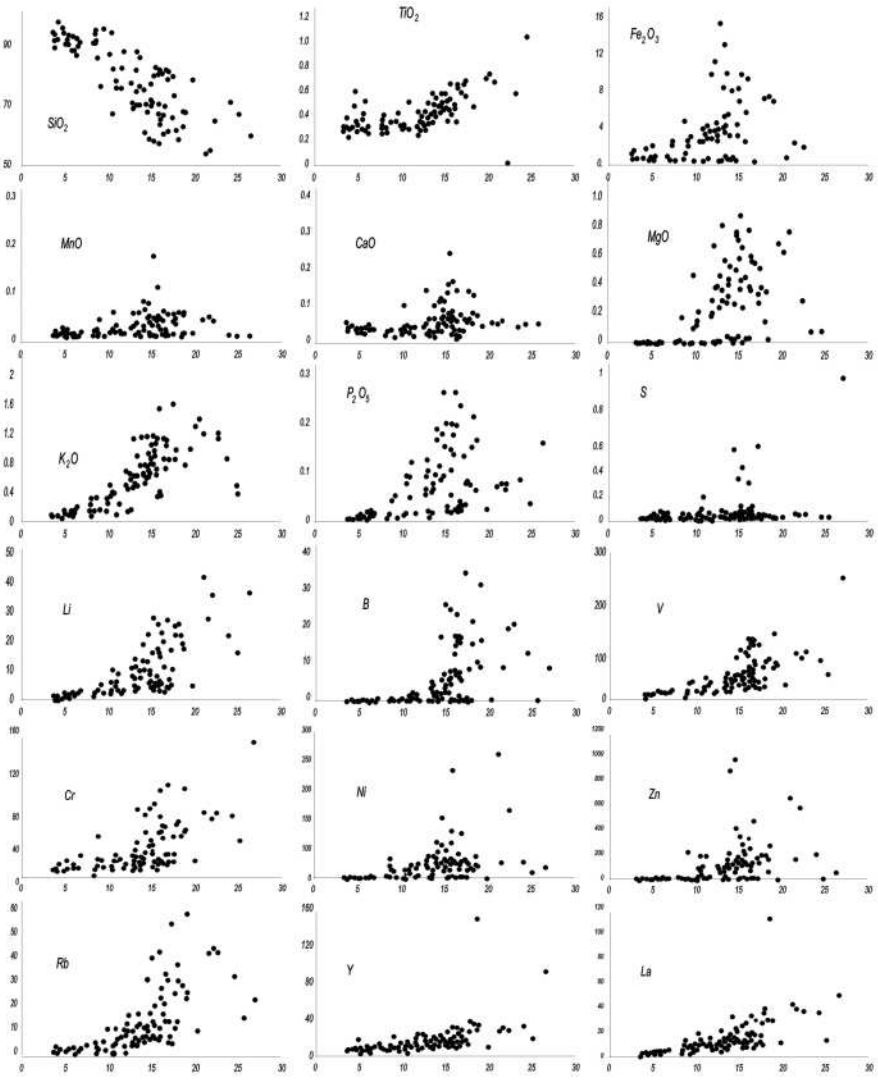


*Fig. 2. Crossplots of analyzed elements vs. $Al_2O_3$.*

1999):

$$Z = \frac{x - \overline{X}}{s}$$

$Z$ = Standardized value derived from original data.
$x$ = Original value.
$X$ = Arithmetic mean.
$s$ = Standard deviation.

Use of standardized values allowed removal of artifacts derived from scale attributes within each set of data, and it equalized the influence of variables with a small variation as opposed to those with a large variation (Crowley *et al*., 1995).

For establishing subdivisions within the section (partitioning into geochemically meaningful zones, i.e., distinctive chemical facies or chemofacies) we choose the cluster-constrained analysis (Gill *et al*., 1993). Multivariate analysis between variables was performed by Multi-Dimensional Scaling (MDS). The package NCSS 2000™ was used in nearly all statistical analysis.

## Results and Interpretation

Geochemical data for the samples from the Mirador Formation at the San Pedro del Rio locality are listed in Table 1. The overall range of compositions for the samples is relatively narrow, and close to the average values for sedimentary rocks (Mason and Moore, 1982); only K and Ca are lightly depleted in the section.

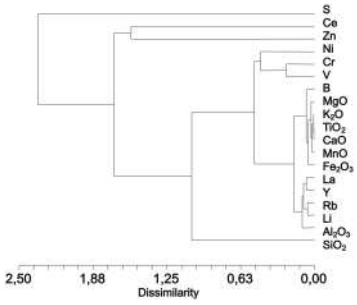


*Fig. 3. Cluster analysis performed in "q" mode on the variables studied in the samples from the Mirador Formation.*

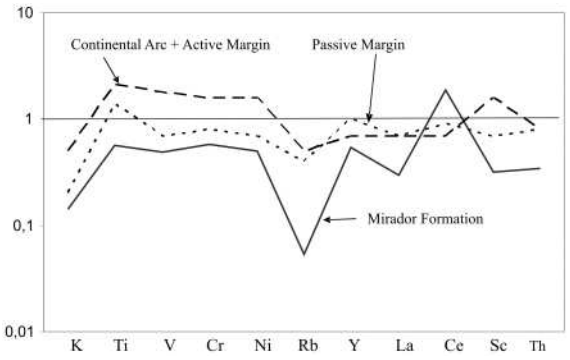


*Fig. 4. Trace-element concentrations, normalized to average upper continental crustal values, in the studied samples (after Wedepohl, 1995) compared to the expected values from passive-margin settings and active-margin settings. The passive margin shows better agreement with most of the elemental enrichments.*

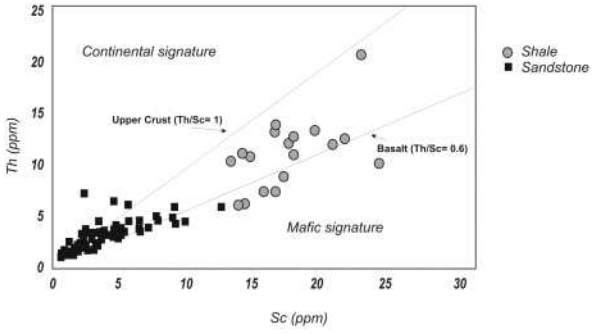


*Fig. 5. Sc-Th crossplot for samples of the Mirador Formation.*

*Sedimentary geochemistry*

A better understanding of trends in the data set is obtained through crossplots of element pairs, where one of the elements is Al or Si (scattergrams of Fralick and Kronberg, 1997). These diagrams allow the evaluation of the mobility or immobility in each element; this behavior is needed to establish the source area composition. As can be seen in Fig. 2, $SiO_2$ shows an opposite trend with $Al_2O_3$, reflecting the differences in hydraulic behavior in sandstones, rich in $SiO_2$, against the fine fraction (i.e., siltstone and shale), where $Al_2O_3$ is enriched. This trend is a measure of sorting in the system, and reflects grain size.

The data presented in Fig. 2 suggest that $TiO_2$ and $K_2O$ are relatively immobile major constituents. Among trace elements, Y, La, Ce (not shown in Fig. 2) and to a lesser extent, Li, Cr, Rb and V, are immobile and affected by sorting in a similar manner; their respective plots form linear arrays along lines extending through the origin. The slight deviations from linearity may be caused by minor differences in source materials, or slight differential hydraulic fractionation of the main mineral phases containing Al or the individual element. On the other hand, MgO, Fe, P, B, Ni and Zn appear highly mobile. MnO, CaO and S are either chemically mobilized or these constituents are added by diagenetic processes (i.e., authigenic mineral formation, cementation).

The immobile elements K, Li and Rb are decisively partitioned during sediment transport, with enrichment in the clay fraction, as can be seen by the high positive correlation with $Al_2O_3$ displayed in the scattergrams (Fig. 2). More horizontal trends for $TiO_2$, La, Ce and Y, reveal a low level of segregation during the sorting process, with little net enrichment in any hydraulic fraction. These elements are likely present in heavy minerals (i.e., monazite, zircon, and rutile). Explanations for the lack of a clear negative trend in the scattergrams for these elements, if they are present as heavy phases enriched in sandstones, include a poor hydraulic sorting, which did not allowed a good fractionation of heavy minerals; or the original small size of these phases in the source rocks allowed preferential deposition in the sandy matrix owing to a high density or possibly as coarse silt with the fine-grained units.

*Elemental relationships*

A clustering procedure was employed to distinguish relationships between elements in the data matrix. Clusters are concentrations of points in space, and two points in the same cluster tend to be more similar than two points in different clusters. Figure 3 shows the results of the cluster analysis in "q mode" applied to the bulk data from the 89 rock samples and 19 variables. Relevant similarities are present in the statistical behavior of the elements in the associations $Al_2O_3$-Li-Rb-Y-La and $Fe_2O_3$-MnO-CaO-$TiO_2$-$K_2O$-MgO-B. Members of both groups are concentrated in the fine fraction, governed by clays (i.e., illite, kaolinite, micas, Fe-rich and trace elements adsorbed onto clays), where the very close association between Li and Rb, and Y with La clearly indicates identical hydraulic partitioning.

*Table 1. Major and trace element concentration for the Mirador Formation sandstones and mudstones (i.e., siltstone and shale)*

| Sample | | Type* | Major elements (wt %) | | | | | | | | Trace elements ($\mu$g/g) | | | | | | | | | | | | | |
|---|---|---|---|---|---|---|---|---|---|---|---|---|---|---|---|---|---|---|---|---|---|---|---|---|
| | | | $SiO_2$ | $Al_2O_3$ | $Fe_2O_3$ | MnO | MgO | CaO | $K_2O$ | $TiO_2$ | TOC** | S | Li | B | Sc | V | Cr | Ni | Zn | Rb | Y | Mo | La | Ce | Th |
| TSPM | 445 | S | 96.84 | 4.19 | 0.22 | <0.01 | <0.01 | 0.04 | 0.09 | 0.25 | <0.002 | <20 | <1 | <1 | 0.7 | 11 | 15 | <1 | <0.5 | 2 | 7 | <1 | 2 | 30 | 1 |
| TSPM | 440 | S | 93.65 | 3.58 | 0.59 | <0.01 | <0.01 | 0.05 | 0.07 | 0.23 | <0.002 | 42 | <1 | <1 | 0.5 | 9 | 8 | <1 | <0.5 | <0.5 | 5 | 2 | 1 | 7 | 1 |
| TSPM | 435 | S | 91.59 | 6.24 | 0.27 | <0.01 | <0.01 | 0.04 | 0.09 | 0.23 | <0.002 | 28 | <1 | <1 | 0.8 | 13 | 13 | <1 | <0.5 | <0.5 | 7 | 2 | 3 | 57 | 2 |
| TSPM | 430 | S | 87.28 | 5.86 | <0.01 | <0.01 | <0.01 | 0.04 | 0.11 | 0.33 | <0.002 | <20 | 1 | <1 | 0.9 | 14 | 15 | <1 | <0.5 | 2 | 8 | <1 | 4 | 58 | 1 |
| TSPM | 425 | S | 93.27 | 8.36 | 0.01 | 0.02 | <0.01 | 0.02 | 0.21 | 0.32 | <0.002 | 27 | 1 | <1 | 1.5 | 13 | 8 | <1 | <0.5 | <0.5 | 6 | <1 | 3 | 41 | 2 |
| TSPM | 420 | S | 87.58 | 11.71 | <0.01 | <0.01 | <0.01 | 0.02 | 0.24 | 0.25 | <0.002 | 43 | 2 | <1 | 1.6 | 16 | 13 | 5 | <0.5 | 1 | 7 | <1 | 4 | 60 | 2 |
| TSPM | 415 | S | 90.37 | 8.31 | <0.01 | 0.01 | <0.01 | 0.02 | 0.16 | 0.26 | <0.002 | 50 | <1 | <1 | 0.6 | 8 | 1 | <1 | <0.5 | 1 | 5 | <1 | 1 | 23 | 1 |
| TSPM | 410 | S | 89.64 | 5.18 | 0.94 | 0.02 | <0.01 | 0.04 | 0.10 | 0.27 | <0.002 | <20 | <1 | <1 | 0.6 | 9 | 9 | <1 | <0.5 | 1 | 5 | <1 | 2 | 36 | 1 |
| TSPM | 405 | S | 93.61 | 4.87 | <0.01 | <0.01 | <0.01 | 0.04 | 0.06 | 0.43 | <0.002 | <20 | <1 | <1 | 0.9 | 10 | 8 | <1 | <0.5 | <0.5 | 17 | 2 | 2 | 31 | 2 |
| TSPM | 400 | S | 88.57 | 3.77 | 0.32 | 0.02 | <0.01 | 0.04 | 0.06 | 0.26 | <0.002 | 24 | <1 | <1 | 0.7 | 9 | 5 | <1 | <0.5 | <0.5 | 6 | <1 | 2 | 35 | 1 |
| TSPM | 395 | S | 91.22 | 3.84 | 1.04 | 0.01 | <0.01 | 0.04 | 0.07 | 0.26 | <0.002 | 35 | <1 | <1 | 0.8 | 10 | 11 | <1 | <0.5 | <0.5 | 5 | 3 | 2 | 28 | 1 |
| TSPM | 390 | S | 92.78 | 3.81 | 0.01 | 0.01 | <0.01 | 0.05 | 0.07 | 0.33 | <0.002 | <20 | <1 | <1 | 1.0 | 10 | 11 | <1 | <0.5 | 1 | 5 | <1 | 2 | 22 | 2 |
| TSPM | 385 | S | 90.78 | 4.20 | <0.01 | 0.02 | <0.01 | 0.05 | 0.07 | 0.18 | <0.002 | <20 | <1 | <1 | 0.5 | 9 | 9 | <1 | <0.5 | 1 | 6 | <1 | 2 | 27 | 1 |
| TSPM | 380 | S | 81.96 | 11.60 | 0.07 | 0.01 | <0.01 | 0.04 | 0.11 | 0.46 | <0.002 | <20 | 1 | <1 | 2.2 | 15 | 11 | <1 | <0.5 | 1 | 12 | 1 | 13 | 146 | 7 |
| TSPM | 375 | M | 70.28 | 23.96 | 0.71 | <0.01 | 0.29 | 0.04 | 1.18 | 0.68 | <0.002 | 86 | 21 | 12 | 15.8 | 79 | 65 | 29 | 193 | 30 | 29 | 7 | 33 | 385 | 14 |
| TSPM | 370 | S | 89.96 | 8.42 | 0.27 | <0.01 | <0.01 | 0.03 | 0.08 | 0.22 | 0.331 | 25 | 1 | <1 | 0.9 | 12 | 10 | 1 | <0.5 | <0.5 | 6 | <1 | 1 | 21 | 2 |
| TSPM | 365 | S | 87.53 | 5.98 | 0.12 | <0.01 | <0.01 | 0.04 | 0.12 | 0.37 | <0.002 | <20 | 1 | <1 | 1.2 | 14 | 11 | <1 | <0.5 | <0.5 | 8 | 2 | 3 | 44 | 2 |
| TSPM | 360 | S | 86.72 | 10.21 | <0.01 | 0.02 | <0.01 | 0.04 | 0.15 | 0.31 | 0.134 | <20 | 1 | <1 | 0.9 | 13 | 11 | <1 | <0.5 | <0.5 | 7 | <1 | 4 | 65 | 2 |
| TSPM | 355 | S | 94.73 | 9.43 | <0.01 | <0.01 | <0.01 | 0.02 | 0.17 | 0.31 | 0.067 | <20 | 1 | <1 | 1.3 | 13 | 12 | <1 | <0.5 | 1 | 7 | <1 | 3 | 58 | 2 |
| TSPM | 350 | S | 92.29 | 5.85 | <0.01 | 0.02 | <0.01 | 0.03 | 0.08 | 0.24 | 0.073 | <20 | 1 | <1 | 1.2 | 11 | 11 | <1 | <0.5 | <0.5 | 7 | <1 | 2 | 44 | 1 |
| TSPM | 345 | S | 78.09 | 16.72 | <0.01 | 0.01 | 0.02 | 0.01 | 0.41 | 0.50 | <0.002 | <20 | 3 | <1 | 4.3 | 34 | 27 | <1 | <0.5 | 7 | 20 | 3 | 17 | 209 | 6 |
| TSPM | 340 | S | 80.63 | 16.86 | <0.01 | <0.01 | 0.02 | 0.03 | 0.38 | 0.38 | <0.002 | 72 | 3 | <1 | 3.2 | 26 | 17 | <1 | <0.5 | 4 | 14 | <1 | 9 | 78 | 4 |
| TSPM | 335 | S | 81.56 | 16.56 | <0.01 | 0.02 | 0.01 | 0.02 | 0.32 | 0.30 | <0.002 | 31 | 2 | <1 | 2.4 | 21 | 14 | 17 | <0.5 | 4 | 11 | <1 | 7 | 62 | 4 |
| TSPM | 330 | S | 93.15 | 10.38 | <0.01 | 0.02 | <0.01 | 0.03 | 0.28 | 0.39 | 0.084 | <20 | 2 | <1 | 2.2 | 18 | 10 | <1 | <0.5 | 3 | 11 | <1 | 8 | 77 | 3 |
| TSPM | 325 | S | 90.23 | 6.70 | 0.53 | 0.02 | <0.01 | 0.04 | 0.21 | 0.22 | <0.002 | <20 | 2 | <1 | 2.3 | 19 | 23 | <1 | <0.5 | 2 | 9 | <1 | 4 | 53 | 2 |
| TSPM | 320 | S | 95.43 | 4.69 | 0.01 | 0.02 | <0.01 | 0.04 | 0.06 | 0.27 | <0.002 | <20 | <1 | <1 | 1.3 | 12 | 15 | <1 | <0.5 | 1 | 6 | <1 | 2 | 23 | 1 |
| TSPM | 315 | S | 91.33 | 5.16 | 0.23 | 0.01 | <0.01 | 0.03 | 0.16 | 0.30 | <0.002 | <20 | <1 | <1 | 1.7 | 11 | 7 | <1 | <0.5 | 1 | 6 | 1 | 3 | 33 | 2 |
| TSPM | 310 | S | 89.81 | 5.14 | 1.02 | <0.01 | <0.01 | 0.04 | 0.10 | 0.55 | <0.002 | 21 | <1 | <1 | 2.1 | 17 | 18 | <1 | <0.5 | <0.5 | 7 | 1 | 3 | 35 | 2 |
| TSPM | 305 | S | 86.38 | 6.29 | 1.49 | <0.01 | <0.01 | 0.03 | 0.09 | 0.48 | <0.002 | 22 | 1 | <1 | 2.1 | 16 | 16 | <1 | <0.5 | 1 | 6 | <1 | 4 | 52 | 2 |
| TSPM | 300 | S | 89.29 | 6.48 | <0.01 | 0.01 | <0.01 | 0.04 | 0.15 | 0.27 | <0.002 | <20 | 1 | <1 | 1.8 | 13 | 11 | <1 | <0.5 | 1 | 7 | <1 | 4 | 47 | 2 |
| TSPM | 295 | S | 90.31 | 8.53 | 0.01 | 0.02 | 0.01 | 0.02 | 0.28 | 0.35 | <0.002 | <20 | 1 | <1 | 1.9 | 19 | 21 | <1 | <0.5 | 2 | 11 | <1 | 7 | 72 | 2 |
| TSPM | 290 | S | 67.35 | 18.57 | 1.87 | 0.01 | 0.34 | 0.05 | 0.99 | 0.62 | <0.002 | 58 | 18 | 9 | 13.9 | 73 | 50 | 26 | 154 | 21 | 27 | <1 | 28 | 296 | 11 |
| TSPM | 285 | S | 61.39 | 17.77 | 6.50 | 0.04 | 0.59 | 0.06 | 1.07 | 0.61 | <0.002 | 173 | 21 | 20 | 15.9 | 82 | 62 | 29 | 193 | 28 | 35 | <1 | 36 | 352 | 13 |
| TSPM | 280 | S | 63.66 | 15.70 | 8.15 | 0.05 | 0.49 | 0.08 | 0.88 | 0.54 | <0.002 | 118 | 16 | 12 | 12.7 | 66 | 50 | 22 | 223 | 21 | 29 | 5 | 26 | 277 | 10 |
| TSPM | 275 | S | 67.17 | 18.71 | 8.99 | 0.06 | 0.51 | 0.13 | 0.86 | 0.53 | 0.341 | 127 | 17 | 15 | 13.5 | 68 | 52 | 24 | 266 | 23 | 32 | 4 | 28 | 287 | 11 |
| TSPM | 270 | S | 60.89 | 16.23 | 9.70 | 0.06 | 0.58 | 0.16 | 0.96 | 0.54 | 0.385 | 169 | 22 | 16 | 16.8 | 76 | 57 | 29 | 329 | 30 | 30 | <1 | 31 | 379 | 12 |
| TSPM | 265 | S | 58.43 | 18.15 | 9.53 | 0.06 | 0.54 | 0.14 | 0.87 | 0.54 | 0.385 | 149 | 25 | 10 | 17.1 | 63 | 45 | 16 | 187 | 26 | 34 | 6 | 29 | 345 | 12 |
| TSPM | 260 | S | 61.3 | 17.74 | 7.77 | 0.05 | 0.58 | 0.06 | 1.10 | 0.58 | 0.319 | 167 | 24 | 14 | 17.0 | 79 | 60 | 22 | 183 | 34 | 26 | 2 | 33 | 374 | 11 |
| TSPM | 255 | S | 64.17 | 22.2 | 6.57 | 0.04 | 0.76 | 0.06 | 1.20 | 0.64 | 0.347 | 218 | 35 | 19 | 18.6 | 94 | 71 | 132 | 561 | 39 | 27 | <1 | 35 | 370 | 13 |
| TSPM | 250 | S | 69.11 | 16.52 | 2.81 | 0.03 | 0.24 | 0.04 | 0.72 | 0.40 | 0.306 | 20 | 10 | <1 | 7.3 | 39 | 25 | 16 | 115 | 12 | 15 | <1 | 11 | 121 | 5 |

| Sample | | Type* | Major elements (wt %) | | | | | | | | Trace elements ($\mu$g/g) | | | | | | | | | | | | | | |
|---|---|---|---|---|---|---|---|---|---|---|---|---|---|---|---|---|---|---|---|---|---|---|---|---|---|
| | | | $SiO_2$ | $Al_2O_3$ | $Fe_2O_3$ | MnO | MgO | CaO | $K_2O$ | $TiO_2$ | TOC** | S | Li | B | Sc | V | Cr | Ni | Zn | Rb | Y | Mo | La | Ce | Th |
| TSPM | 245 | M | 54.76 | 21.61 | 7.09 | 0.05 | 0.62 | 0.05 | 1.38 | 0.69 | <0.002 | 210 | 27 | 18 | 20.7 | 83 | 63 | 33 | 150 | 40 | 30 | <1 | 37 | 392 | 12 |
| TSPM | 240 | M | 54.17 | 21.07 | 6.84 | 0.04 | 0.68 | 0.06 | 1.29 | 0.67 | 0.329 | 388 | 41 | 8 | 20.0 | 92 | 72 | 249 | 631 | 39 | 26 | 3 | 40 | 412 | 12 |
| TSPM | 235 | S | 80.27 | 16.12 | 0.01 | 0.02 | 0.04 | 0.02 | 0.89 | 0.41 | 0.329 | 73 | 4 | <1 | 4.7 | 27 | 16 | <1 | <0.5 | 12 | 13 | <1 | 11 | 132 | 3 |
| TSPM | 230 | S | 78.66 | 17.29 | 0.01 | 0.02 | 0.03 | 0.08 | 0.86 | 0.45 | <0.002 | <20 | 4 | <1 | 4.3 | 26 | 16 | <1 | <0.5 | 9 | 15 | <1 | 12 | 143 | 4 |
| TSPM | 225 | S | 80.38 | 15.64 | 0.43 | 0.01 | 0.03 | 0.04 | 0.79 | 0.43 | 0.022 | 406 | 3 | <1 | 4.7 | 29 | 20 | <1 | <0.5 | 10 | 13 | <1 | 12 | 136 | 4 |
| TSPM | 220 | S | 82.22 | 15.33 | 0.01 | 0.01 | 0.02 | 0.06 | 0.68 | 0.44 | <0.002 | <20 | 3 | <1 | 3.7 | 22 | 18 | <1 | <0.5 | 6 | 14 | <1 | 10 | 99 | 3 |
| TSPM | 215 | S | 67.04 | 24.95 | 1.68 | 0.01 | 0.07 | 0.05 | 0.85 | 0.53 | <0.002 | 149 | 15 | <1 | 8.6 | 49 | 40 | 10 | <0.5 | 14 | 18 | <1 | 13 | 168 | 6 |
| TSPM | 210 | S | 77.82 | 19.76 | 0.01 | 0.02 | 0.03 | 0.05 | 0.79 | 0.42 | <0.002 | 169 | 4 | <1 | 4.5 | 29 | 16 | <1 | <0.5 | 9 | 11 | <1 | 10 | 106 | 3 |
| TSPM | 205 | S | 81.56 | 13.12 | 0.01 | 0.02 | 0.02 | 0.05 | 0.44 | 0.31 | <0.002 | 28 | 4 | <1 | 3.2 | 19 | 20 | <1 | <0.5 | 5 | 8 | <1 | 7 | 81 | 2 |
| TSPM | 200 | S | 87.54 | 13.16 | 0.01 | 0.01 | 0.01 | 0.03 | 0.43 | 0.36 | <0.002 | <20 | 3 | <1 | 2.4 | 18 | 16 | <1 | <0.5 | 5 | 9 | <1 | 5 | 71 | 2 |
| TSPM | 195 | S | 79.43 | 15.23 | 0.01 | 0.01 | 0.03 | 1.18 | 0.60 | 0.45 | <0.002 | <20 | 3 | <1 | 3.4 | 21 | 12 | <1 | <0.5 | 6 | 10 | 1 | 9 | 124 | 3 |
| TSPM | 190 | S | 85.49 | 13.57 | 0.01 | 0.02 | 0.01 | 0.07 | 0.53 | 0.39 | <0.002 | 57 | 3 | <1 | 3.0 | 21 | 12 | <1 | <0.5 | 6 | 10 | <1 | 7 | 104 | 2 |
| TSPM | 185 | S | 85.71 | 8.71 | 1.5 | 0.01 | 0.01 | 0.03 | 0.16 | 0.26 | 0.423 | 12005 | 2 | <1 | 2.7 | 34 | 48 | 15 | <0.5 | 2 | 20 | 3 | 13 | 180 | 3 |
| TSPM | 180 | S | 93.78 | 8.41 | 0.01 | 0.02 | <0.01 | 0.03 | 0.29 | 0.27 | <0.002 | <20 | 2 | <1 | 1.6 | 18 | 17 | <1 | <0.5 | 3 | 7 | <1 | 3 | 84 | 2 |
| TSPM | 175 | S | 92.99 | 5.20 | 0.01 | 0.01 | <0.01 | 0.04 | 0.14 | 0.22 | <0.002 | <20 | 1 | <1 | 2.9 | 14 | 11 | <1 | <0.5 | 2 | 7 | <1 | 2 | 85 | 2 |
| TSPM | 170 | M | 59.81 | 26.39 | 1.17 | 0.01 | 0.07 | 0.05 | 0.43 | 0.99 | 0.280 | 8770 | 36 | 8 | 21.9 | 243 | 151 | 20 | 47 | 20 | 91 | 28 | 47 | 593 | 20 |
| TSPM | 165 | M | 62.61 | 18.46 | 5.34 | 0.01 | 0.27 | 0.05 | 1.61 | 0.63 | 0.122 | 11022 | 21 | 29 | 23.2 | 129 | 99 | 40 | 67 | 53 | 147 | 10 | 107 | 1260 | 10 |
| TSPM | 160 | M | 58.69 | 14.65 | 10.97 | 0.08 | 1.08 | 0.11 | 1.16 | 0.54 | 0.278 | 2540 | 21 | 24 | 15.8 | 97 | 77 | 117 | 958 | 37 | 20 | 2 | 20 | 243 | 7 |
| TSPM | 155 | M | 60.86 | 14.04 | 9.74 | 0.08 | 0.79 | 0.10 | 0.89 | 0.46 | 0.320 | 4240 | 18 | 16 | 13.5 | 83 | 69 | 72 | 863 | 27 | 18 | 4 | 31 | 332 | 6 |
| TSPM | 150 | M | 60.60 | 16.82 | 7.75 | 0.06 | 1.22 | 0.14 | 1.52 | 0.62 | 0.199 | 4510 | 26 | 32 | 16.3 | 115 | 105 | 90 | 478 | 49 | 26 | <1 | 28 | 322 | 9 |
| TSPM | 145 | M | 57.74 | 15.20 | 15.17 | 0.18 | 1.45 | 0.11 | 1.15 | 0.51 | 0.474 | 3250 | 27 | 23 | 15.1 | 96 | 82 | 55 | 340 | 39 | 24 | 7 | 23 | 261 | 7 |
| TSPM | 140 | S | 66.69 | 10.53 | 4.24 | 0.06 | 0.46 | 0.10 | 0.51 | 0.28 | 0.061 | 619 | 9 | <1 | 4.5 | 40 | 25 | 17 | 182 | 9 | 11 | 4 | 11 | 147 | 4 |
| TSPM | 135 | S | 68.92 | 12.84 | 3.31 | 0.06 | 0.29 | 0.04 | 0.67 | 0.38 | <0.002 | 317 | 7 | <1 | 4.4 | 41 | 30 | 34 | 97 | 9 | 16 | 1 | 12 | 189 | 4 |
| TSPM | 130 | S | 70.75 | 12.88 | 1.88 | 0.03 | 0.19 | 0.05 | 0.15 | 0.21 | <0.002 | 95 | 6 | <1 | 1.9 | 20 | 15 | 20 | 64 | 3 | 9 | 2 | 4 | 83 | 2 |
| TSPM | 125 | S | 72.82 | 17.49 | 2.53 | 0.06 | 0.36 | 0.04 | 0.74 | 0.31 | <0.002 | 204 | 9 | <1 | 5.1 | 41 | 27 | 14 | 125 | 12 | 13 | 3 | 9 | 165 | 3 |
| TSPM | 120 | S | 69.85 | 13.62 | 3.59 | 0.06 | 0.45 | 0.02 | 0.60 | 0.27 | <0.002 | 234 | 9 | 1 | 4.3 | 35 | 23 | 15 | 69 | 10 | 12 | <1 | 7 | 78 | 3 |
| TSPM | 115 | S | 76.78 | 9.01 | 1.85 | 0.04 | 0.17 | 0.04 | 0.32 | 0.22 | <0.002 | 199 | 5 | <1 | 2.4 | 34 | 17 | 13 | 211 | 5 | 9 | 3 | 7 | 110 | 3 |
| TSPM | 110 | S | 69.74 | 13.12 | 2.71 | 0.04 | 0.67 | 0.14 | 0.42 | 0.24 | 0.056 | 307 | 13 | 5 | 3.3 | 50 | 39 | 16 | 81 | 15 | 14 | 1 | 12 | 137 | 3 |
| TSPM | 105 | S | 66.97 | 15.65 | 3.52 | 0.05 | 0.27 | 0.14 | 0.79 | 0.38 | 0.095 | 417 | 7 | <1 | 6.2 | 35 | 17 | 3 | 18 | 7 | 11 | 3 | 7 | 96 | 4 |
| TSPM | 100 | S | 75.77 | 13.56 | 2.38 | 0.01 | 0.24 | 0.03 | 0.48 | 0.25 | <0.002 | 77 | 7 | <1 | 3.4 | 39 | 18 | 8 | 17 | 5 | 11 | 3 | 7 | 99 | 3 |
| TSPM | 095 | S | 77.00 | 12.67 | 1.83 | 0.03 | 0.19 | 0.04 | 0.48 | 0.26 | <0.002 | 64 | 10 | <1 | 2.3 | 28 | 24 | 23 | 93 | 5 | 10 | 2 | 6 | 81 | 2 |
| TSPM | 090 | S | 75.34 | 10.88 | 1.24 | 0.03 | 0.15 | 0.05 | 0.44 | 0.25 | <0.002 | 30 | 5 | <1 | 2.2 | 27 | 18 | 9 | 14 | 5 | 10 | 2 | 9 | 109 | 3 |
| TSPM | 085 | S | 74.43 | 13.16 | 2.71 | 0.04 | 0.39 | 0.05 | 0.62 | 0.29 | <0.002 | 38 | 10 | 2 | 5.0 | 53 | 75 | 47 | 92 | 11 | 13 | 2 | 13 | 143 | 4 |
| TSPM | 080 | S | 74.52 | 14.10 | 2.26 | 0.03 | 0.36 | 0.07 | 0.61 | 0.30 | <0.002 | 46 | 9 | <1 | 4.3 | 48 | 26 | 21 | 103 | 9 | 15 | 2 | 10 | 143 | 4 |
| TSPM | 075 | S | 76.62 | 14.87 | 2.17 | 0.04 | 0.39 | 0.06 | 0.67 | 0.31 | <0.002 | <20 | 8 | 2 | 4.5 | 46 | 26 | 18 | 44 | 11 | 12 | <1 | 12 | 148 | 4 |
| TSPM | 070 | S | 70.65 | 15.76 | 3.39 | 0.03 | 0.74 | 0.17 | 0.87 | 0.41 | 0.111 | 349 | 15 | 7 | 8.5 | 60 | 98 | 93 | 151 | 21 | 17 | 2 | 15 | 190 | 5 |
| TSPM | 065 | S | 65.81 | 17.30 | 3.71 | 0.04 | 0.76 | 0.08 | 1.13 | 0.42 | <0.002 | 115 | 16 | 8 | 9.3 | 65 | 44 | 36 | 162 | 23 | 16 | <1 | 16 | 199 | 4 |
| TSPM | 060 | S | 67.72 | 14.41 | 3.11 | 0.05 | 0.56 | 0.05 | 0.78 | 0.38 | <0.002 | 268 | 12 | 7 | 6.2 | 51 | 34 | 27 | 118 | 15 | 14 | 1 | 14 | 157 | 4 |
| TSPM | 055 | S | 65.30 | 15.90 | 4.74 | 0.05 | 0.73 | 0.25 | 0.78 | 0.40 | 0.106 | 636 | 14 | 15 | 7.4 | 63 | 51 | 220 | 142 | 15 | 14 | 2 | 11 | 145 | 5 |
| TSPM | 050 | S | 56.85 | 15.75 | 12.83 | 0.11 | 2.11 | 0.16 | 1.04 | 0.46 | 0.335 | 2320 | 25 | 16 | 13.2 | 123 | 69 | 69 | 208 | 25 | 18 | 2 | 17 | 233 | 6 |

*Table 1. (continued)*

| Sample | | Type* | Major elements (wt %) | | | | | | | | Trace elements (μg/g) | | | | | | | | | | | | | |
|---|---|---|---|---|---|---|---|---|---|---|---|---|---|---|---|---|---|---|---|---|---|---|---|---|
| | | | $SiO_2$ | $Al_2O_3$ | $Fe_2O_3$ | MnO | MgO | CaO | $K_2O$ | $TiO_2$ | TOC** | S | Li | B | Sc | V | Cr | Ni | Zn | Rb | Y | Mo | La | Ce | Th |
| TSPM | 045 | S | 66.67 | 16.34 | 5.36 | 0.04 | 0.88 | 0.09 | 1.10 | 0.48 | <0.002 | 224 | 19 | 16 | 11.9 | 69 | 56 | 52 | 247 | 28 | 23 | 1 | 18 | 234 | 6 |
| TSPM | 040 | S | 70.66 | 15.01 | 3.41 | 0.03 | 0.52 | 0.09 | 0.78 | 0.35 | <0.002 | 236 | 15 | 5 | 6.7 | 50 | 36 | 36 | 163 | 18 | 12 | 1 | 9 | 127 | 4 |
| TSPM | 035 | S | 66.24 | 16.00 | 3.80 | 0.03 | 0.70 | 0.07 | 0.90 | 0.39 | 0.090 | 362 | 15 | 7 | 8.7 | 59 | 44 | 23 | 102 | 19 | 20 | <1 | 16 | 222 | 4 |
| TSPM | 030 | S | 81.29 | 10.44 | 0.92 | 0.03 | 0.11 | 0.04 | 0.26 | 0.28 | <0.002 | <20 | 5 | <1 | 2.6 | 22 | 17 | 10 | 84 | 4 | 13 | <1 | 12 | 179 | 3 |
| TSPM | 025 | S | 77.70 | 10.82 | 1.43 | 0.02 | 0.15 | 0.03 | 0.34 | 0.28 | <0.002 | <20 | 4 | 2 | 3.1 | 26 | 21 | 9 | 2 | 5 | 9 | <1 | 8 | 104 | 3 |
| TSPM | 020 | S | 69.67 | 14.79 | 3.84 | 0.02 | 0.44 | 0.12 | 0.62 | 0.38 | <0.002 | 404 | 9 | 3 | 6.1 | 49 | 41 | 33 | 394 | 12 | 12 | 2 | 12 | 166 | 4 |
| TSPM | 015 | S | 69.91 | 14.04 | 3.10 | 0.03 | 0.29 | 0.03 | 0.51 | 0.33 | <0.002 | 108 | 12 | 1 | 5.3 | 40 | 49 | 41 | 197 | 10 | 12 | 3 | 11 | 170 | 4 |
| TSPM | 010 | S | 75.24 | 11.16 | 2.24 | 0.02 | 0.22 | 0.04 | 0.41 | 0.27 | <0.002 | 47 | 8 | 1 | 3.5 | 33 | 20 | 26 | 196 | 6 | 11 | <1 | 8 | 112 | 4 |
| TSPM | 005 | S | 71.72 | 14.82 | 2.63 | 0.02 | 0.32 | 0.03 | 0.51 | 0.44 | <0.002 | 25 | 9 | 4 | 5.3 | 41 | 29 | 15 | 63 | 6 | 12 | <1 | 13 | 161 | 6 |
| G-2 | | cert | 69.14 | 15.39 | 2.66 | 0.03 | 0.75 | 1.96 | 4.48 | 0.48 | | 100 | 34 | 2 | 3.5 | 36 | — | 5 | 86 | 170 | 11 | 1 | 89 | 160 | 25 |
| G-2 | | | 69.91 | 15.16 | 2.59 | 0.04 | 0.70 | 2.01 | 4.55 | 0.45 | | 106 | 38 | <1 | 3.0 | 30 | — | 6 | 94 | 159 | 14 | <1 | 95 | 164 | 29 |
| AGV1 | cert | | 58.84 | 17.15 | 6.77 | 0.09 | 1.53 | 4.94 | 2.92 | 1.05 | — | — | 12 | 8 | 11.8 | 120 | 10 | 16 | 88 | 67 | 19 | 3 | 38 | 67 | 6 |
| AGV1 | | | 57.71 | 17.20 | 6.71 | 0.08 | 1.48 | 5.03 | 2.89 | 1.05 | — | — | 11 | 9 | 10.9 | 118 | 9 | 13 | 85 | 60 | 18 | 2 | 36 | 69 | 5 |

* = *Lithology; S = sandstone; M = mudstone.*
** = *Total Organic Carbon, expressed as % w/w.*

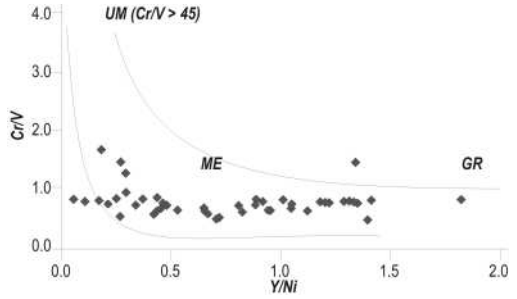


*Fig. 6. Hiscott Diagram (Cr/V vs. Y/Ni), allowing the discrimination between ultramafic (UM), felsic metamorphic (ME) and granitic (GR) source composition (after Hiscott, 1984).*

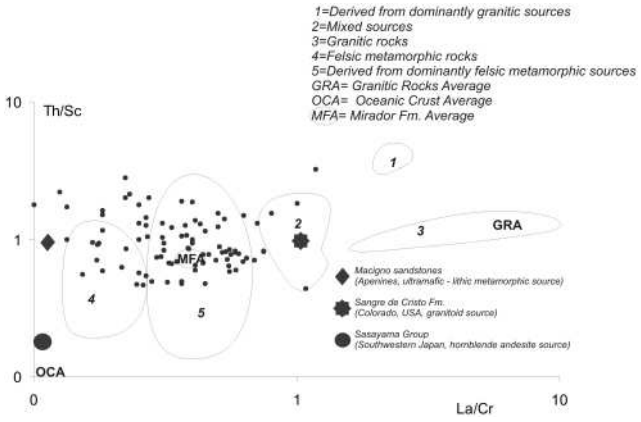


*Fig. 7. Th/Sc vs. La/Cr discrimination diagram (after Piovano et al., 1999) applied to the Mirador Formation. Values of Macigno, Sangre de Cristo and Sasayama Fms from Dinelli et al. (1999), Cullers (2000) and Asiedu et al. (2000).*

Transition elements (V, Cr, Mo, Ni and Zn) together with Ce and S show no remarkable associations. This result suggests that factors other than hydraulic, physical partitioning (e.g., post-depositional redox conditions) are governing their distribution. The particular case of $SiO_2$, with a high dissimilarity coefficient (Fig. 3), is a natural consequence of its enrichment in the sand-sized fraction, and consequent depletion in the finer-grained samples. Therefore, this variable has an opposite trend to the rest.

*Tectonic setting*

The concentration of selected major and trace elements, normalized to average upper continental crustal values (after Wedepohl, 1995) are compared to expected values from passive- and active-margin settings and plotted on a logarithmic scale in Fig. 4. This approach is suitable for inferring the tectonic setting. Comparison of the average Mirador Formation to a passive margin setting

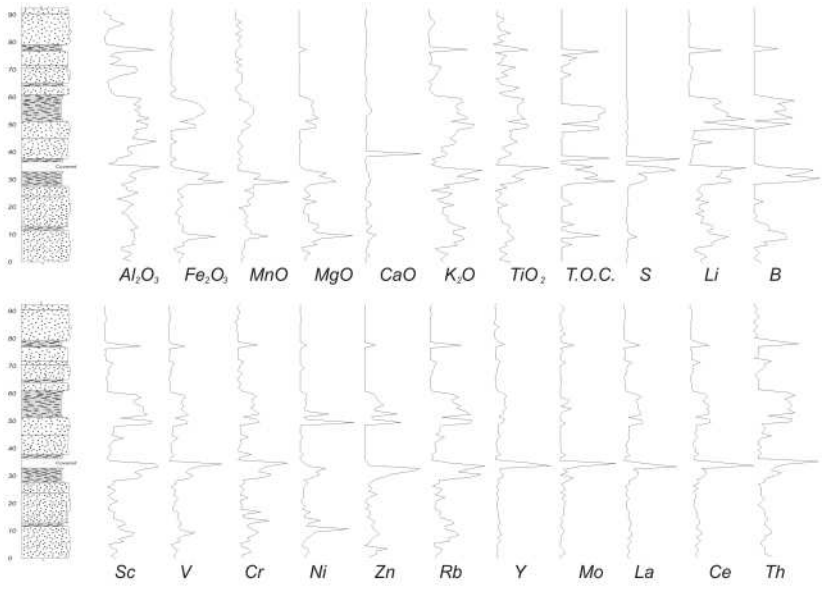


*Fig. 8. Chemostratigraphic profiles for the determined major and trace elements in the Mirador Formation.*

reveals a better agreement (Fig. 4) than with an active margin and a continental arc setting. The $K_2O$-V-Cr-Ni depletions are similar, and trends in Rb-Y-La are comparable in shape and of the same order of magnitude. However, this graphic does not provide a strong difference between the three curve shapes. The depletion in the studied elements, in comparison with both passive and active margin trends in Fig. 4, reflects the predominantly coarse, sandstone composition.

*Provenance*

Trace-element data were also plotted on a Sc-Th scatter diagram (Fig. 5). The samples generally cluster along a nearly straight trend situated between continental and mafic domains. Sandstone samples are depleted both in Sc and Th and fall in the lower left corner. However, shale samples occupy a field in the plot that is consistent with a source of intermediate composition.

On a Y/Ni vs. Cr/V diagram (Hiscott, 1984), ultramafic source rocks plot with low Y/Ni and high Cr/V, while felsic source rocks plot with lower Cr/V and higher Y/Ni ratios (Fig. 6). Felsic metamorphic rocks appear in an intermediate field. Upper and lower curves represent the mixing lines of ultramafic (Cr/V = 45, Y/Ni = 0.001), felsic metamorphic (Cr/V = 1.23, Y/Ni = 1.02) and granitic rocks (Cr/V = 0.25, Y/Ni = 2.33). On Fig. 6, the majority of samples plot near or around the felsic metamorphic field. Samples in this diagram show constancy in Cr/V ratio; on the other hand, the Y/Ni ratio varies considerably. This behavior could be the result of a further sediment source: recycled sedimentary rocks. As a consequence of recycling processes, Ni may be preferentially depleted from sediments, increasing the Y/Ni ratio and promoting the scattering in the values; Y, Cr and V are immobile and affected by sorting in a similar way, as previously described.

A second plot, proposed by Piovano *et al*. (1999) shows the Th/Sc vs. La/Cr variability for the Mirador Fm (Fig. 7). This diagram allows the discrimination of source rocks based in a felsic (rich in Th and La, depleted in Sc and Cr, thus high Th/Sc and La/Cr ratios) or mafic affinity (low Th/Sc and La/Cr ratios). In this diagram, felsic metamorphic sources yield sediments with lower Th/Sc and La/Cr, whereas granitoid rocks exhibit higher values. Fields showed in this graphic are the same as in Piovano *et al*. (1999). In Fig. 7, samples from the Mirador Formation appear mainly in felsic metamorphic or derived from felsic metamorphic fields. This result is in agreement with that obtained from Fig. 6. The geochemical interpretation of provenance, derived from plots such as these, however, must be viewed with caution, because of its great oversimplification: fields for metamorphic rocks, or recycled sediments are not clear. Piovano *et al*. (1999) demonstrated that Cr/Th, La/Cr, Th/Sc and, to a lesser extent, Sm/Nd, exhibit significant differences in both groups of source rocks (i.e., metamorphic and granitic). Petrographic features of sandstones are the key to the confirmation of provenance determination derived by geochemical criteria (Dinelli *et al*., 1999). In fact, the presence of muscovite, epidote and staurolite, together with poly-crystalline quartz, is strongly indicative of a metamorphic source, in agreement with results from Figs. 6 and 7.

*Chemostratigraphy*

Analyzed elements were plotted against a detailed lithologic log for the total thickness of the Mirador Formation in the study area to illustrate relationships between sediment type and geochemical composition. A summary of the chemostratigraphic profiles from the Mirador Formation (Fig. 8) indicates a series of characteristic excursions and trends. Strong changes in trends (i.e., sharp increases in elemental concentration) for several geochemical profiles obtained from the Mirador Formation are coincident, or nearly so at the same stratigraphic level (approximately 35 and 63 m measured from the bottom of the unit). Other minor variations were also detected, at different heights. These changes delineate boundaries between zones or intervals of the section with a similar geochemical behavior or composition; such intervals are chemofacies. Some boundaries coincide broadly with lithologic boundaries, but other geochemical changes are situated in places not coincident with relevant or abrupt contacts (e.g., transitions from coarse sandstone to shale).

It is difficult to precisely delineate boundaries between chemofacies, or define the number of distinctive chemofacies in the chemostratigraphic profile. However, multivariate statistics can help in this task: evaluating different multivariate methods, the most appropriate for this task was found to be the "cluster constrained technique" (Gill *et al*., 1993). The technique used here is the incremental sum of squares mode or Ward's Minimum Variance, in which groups are formed so that the pooled within-group sum of squares is minimized. The results of the clustering are portrayed as a dendrogram, a hierarchical structure of nested affiliations between intermediate divisions at various hierarchical levels. The special requirements of the stratigraphic context of the zonation are observed by the addition of an adjacency constraint, which prohibits the merger of individual depth levels or lower order clusters if their members are not vertically contiguous.

Applying the cluster constrained technique to the data from the Mirador Formation, a constrained dendrogram is obtained (Fig. 9). The number of final groups defined by the dendrogram is a function of the selection of a suitable cutoff (Gill *et al*., 1993). For this situation, two major groups are distinctive in the unit, with a boundary between 62 and 63 m in stratigraphic height. Minor divisions are present at 38–39, 51–52 and 79–80 m. Thus, a total of three boundaries defining 4 chemical facies or chemofacies can be determined, assuming a cutoff of approximately 0.7 (the x-axis in the dendrogram is an arbitrarily dimensionless dissimilarity index).

Chemofacies M1 corresponds to the bottom of the unit, between 0 and 38 meters, comprising the first lithological association $S_1$ and 2/3 of the following lithological association $Sh_1$. It is mainly a sandy section, with moderate sorting, and the matrix is present to a lesser extent (5–10%). In the profiles (Fig. 8) the most conspicuous geochemical features are relative high concentrations of $K_2O$, MgO, CaO and P, in relation to the upper divisions. On the other hand, depletion in Y, $TiO_2$, Mo and Cr is evident in the profiles.

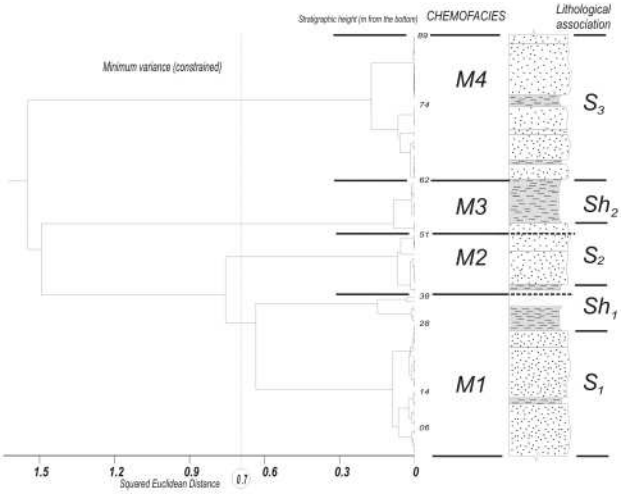


*Fig. 9. Cluster constrained analysis performed on the samples, in their stratigraphic position, with the derived chemofacies. A cut-off value of 0.7 was chosen.*

Chemofacies M2 is defined between 39 and 51 m. This section, overlaying M1 is composed of quartz-sandstones and lithic sandstones and comprises the upper lithological association $Sh_1$ and nearly all $S_2$. The bottom of the basal conglomeratic sandstone shows a clear cut and fill-structure, revealing an erosional episode. In the chemical profiles (Fig. 8), the most remarkable feature is a depletion in the concentrations of MnO, MgO, Ni, Zn and P, in comparison to the underlying chemofacies.

The vertical extent of the third chemofacies, M3, is 10 meters, from 52 to 62 m in the stratigraphic log. This chemofacies comprises all the $Sh_2$ lithological association, and the upper part of the underlying $S_2$ In contrast with chemofacies M1 and M2, the lithology of this interval is dominated by very fine-grained, gray sandstones, sandy siltstones, siltstones and shales. The higher organic matter content is evidenced by the prevailing dark color.

Chemofacies M4 begins at 63 m in the log and ends at the top of the section, at the contact with the uppermost Carbonera Formation. This interval matches with the lithological association $S_3$. A prominent feature of this interval is the presence of conglomeratic sandstones, interlayered with thin shales showing flaser stratification; some coaly lenses are present at the bottom of this chemofacies. Some sandstone bodies, mainly in the top

of the sequence were petrographically classified as quartz-arenites. Geochemical trends are delineated by a general depletion in several elements, mainly as a consequence of the absolute increase in $SiO_2$.

All changes in the last chemofacies contrast with all the other chemical divisions described. This fact is the result of a compositional change in the sandstone bodies, mainly quartz-arenites, free from lithic fragments, and absence of matrix. Thus, all trace elements (and many major chemical components also) are "diluted" in $SiO_2$, thereby causing the typical profiles shown in Fig. 8. This result evidences a drastic change in chemical conditions. Mixed combinations of source changes and/or environment conditions were present during sedimentation of this chemofacies.

Quartz-arenite is the result of re-working in the sediments, where the compositional and textural maturity are high, like beach or eolian deposits, or barrier sand bodies in the architectural arrangement of an estuarine facies model (Dalrymple *et al*., 1992). Thus, the origin of this chemofacies can be seen as a result of an environmental change, with the deposition of "clean" sand-size sediments reflecting a higher degree of compositional maturity.

*Chemostratigraphic interpretation of provenance changes*

Several geochemical indices reflecting changes of provenance during deposition of the Mirador Formation can be employed to further analyze the data. These are indices which have higher concentrations in source terrains with mafic rock elements (Cr, Sc, Ni) relative to immobile, incompatible elements more abundant in felsic source terrains (Li, Th, Ce, Y, La). For example, the index Y/Ce represents a chemical signature, which should be constant during a given time span if no change in source composition occurred. When a geochemically different supply of clastic sediments appears, the value of the original index must change to reflect the new source if its relative proportion is significant. For the example given here, only felsic-mafic composition changes in the source will be detected. This relationship (Y/Ce, Fig. 10-a) seems to suggest that only the last chemofacies exhibits a change in source composition. The remarkable constancy in the Y/Ce profile is diagnostic of a homogeneous source input during the Mirador Formation deposition of chemofacies M1–M3. The La/Cr profile (Fig. 10-b) is essentially constant through the log, with a weak decrease towards the top, possibly revealing a gradual change in source composition. The relative decrease in nearly all elements in this last chemofacies (Fig. 8), together with the increase in Y/Ce suggests a change in the sediment supply, modifying the chemical signature of the unit. The Th/Sc ratio (Fig. 10-c) exhibits a notable increase towards the top of the unit, just when the chemofacies M4 appears; higher values for this ratio, not affected by lithological changes, reveal a more felsic character for the source. Thus, the last chemofacies is a result not only of a change in depositional environment or energy conditions, but also of a change in the source composition. The probability of a para-conformity or hiatus is not discarded, because of the simultaneous change in lithological features of sandstones, in chemical composition, in environmental conditions of deposition and changes in source composition. In the field, a cut-and fill structure is present at the boundary between the lithological associations $Sh_2$ and $S_3$, at the bottom of the sandstone bed. The coincidence of simultaneous changes in chemical attributes in a single point of the log (e.g., provenance, redox conditions, and environment) may be an indicative marker of an interruption of the sedimentary record. Other evidence pointing to an unconformity is given by the coincidence between the lithological change in the field (contact between $Sh_2$ and $S_3$) and the chemostratigraphic boundary M3–M4 (Fig. 9). In an uninterrupted sedimentary succession, chemical changes are present before the lithological ones, because of the higher sensitivity of trace element composition towards these processes (redox, climate, and provenance) than macroscopic lithological attributes. In the Mirador Formation, nearly all the boundaries between chemofacies appear at least 1 m before a lithological change (M1–M2 boundary is present before the $Sh_1$–$S_2$ transition; M2–M3 boundary appears before the $S_2$–$Sh_2$ transition). On the contrary, the boundary between chemofacies M3 and M4 coincides with the $Sh_2$–$S_3$ contact; strongly suggesting an interruption in the sedimentary record.

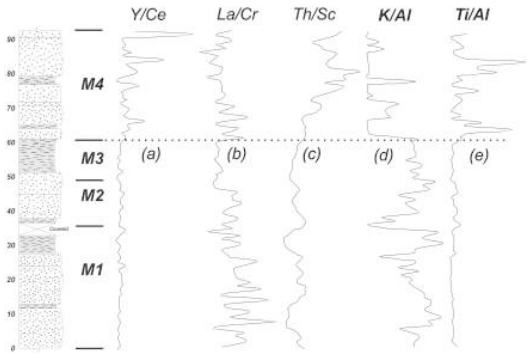


*Fig. 10. Chemostratigraphic profiles for five assayed relationships. a) Y/Ce; b) La/Cr; c) Th/Sc; d) K/Al and e) Ti/Al. See interpretation in text.*

*Chemostratigraphic interpretation of climate, redox and marine influence*

Besides provenance, other clues can be inferred using chemostratigraphic profiles. $K_2O/Al_2O_3$ and $TiO_2/Al_2O_3$

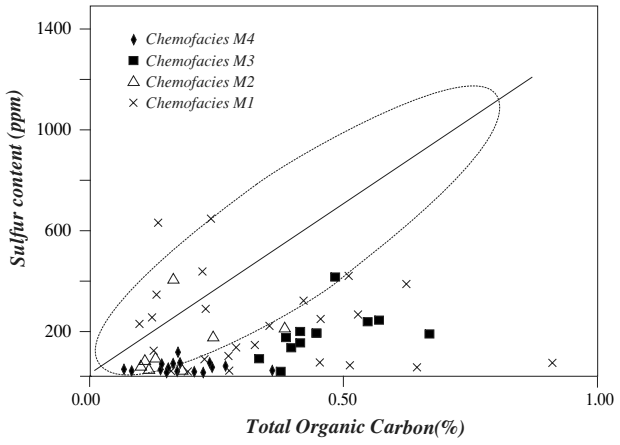


*Fig. 11. Berner diagram (TOC vs. S) for samples from the Mirador Formation. Each chemofacies is plotted separately.*

ratios can be used as paleoclimatic indicators, based on the relative proportion of a mobile vs. an immobile element (K and Al), whereas for the second ratio, one utilizes the preferential tendency of $TiO_2$ in heavy, non-silicate mineral phases (as rutile), which preferentially are transported by air (eolian process) and therefore indicative of arid conditions, vs. $Al_2O_3$ which serves as an indicator of clay genesis, in humid conditions (Yarincik and Murray, 2000; Reinhardt and Ricken, 2000; Bhatt, 1974).

For the uppermost chemofacies M4, a significant decrease in $K_2O/Al_2O_3$ is detected in the profile (Fig. 10-c) suggesting more humid conditions at the end of the Mirador Formation, with respect to the other chemofacies. However, this result is not in agreement with the $TiO_2/Al_2O_3$ profile (Fig. 10-d), which suggests an opposite trend in paleoclimatic conditions. For instance, variations observed in $K_2O/Al_2O_3$ and $TiO_2/Al_2O_3$ may be a direct consequence of the $SiO_2$ increase, revealing strong compositional changes in the sandstone bodies and therefore changes in provenance and/or environment, as previously described rather than a result of climatic control on chemical composition. This is an excellent example of how the chemical behavior of the elements can be influenced by more than one process (i.e., $K_2O$ variation due to changes in provenance, climate, or both).

The mainly sandy character of the studied unit, strongly limits the ability to detect important redox variations. In the fine to medium-grained sediment intervals (shales and siltstones), some trends associated with redox variations are observed, e.g., the relative decrease in MnO (the reduced form, $Mn^{++}$, is soluble and therefore, leached from the sediment), together with a relative increase in TOC and Mo. Nevertheless, no correlation between TOC, MnO or Mo was detected in the studied unit.

Paleosalinity-related elements (B, S) can be useful to constrain variations in the marine influence (Banerjee and Goodarzi, 1990). The positive correlation between TOC and S is a primary signal of marine deposition (Berner, 1983) and is weakly present only in the first and second chemofacies, but absent in the upper two (Fig. 11). The boron profile in Fig. 8 is only evident at levels with mudstone, due the very low content of this element in sandstone. The boron content decreases from the shale beds ($Sh_1$, with a top value of 32 $\mu$g/g B) at the upper part of chemofacies M1 until the last shale layer at the middle chemofacies M4 (12 $\mu$g/g B). Two independent geochemical indicators, the Berner plot (TOC vs. S, Fig. 11) and the boron content, suggest a more marine influence for chemofacies M1. In the following chemofacies, all marine indicators are virtually absent.

## SUMMARY

Integration of geochemical and chemostratigraphic analyses, along with petrographic and field observations, indicate the following:

- The chemical signature of the Mirador Formation is consistent with a passive tectonic margin, with the Guyana shield as a potential source for the sediments of this unit.
- Elemental ratios and geochemical diagrams fall within the range of a felsic composition provenance, suggesting a granitoid composition. Petrographic interpretation of the sandstones suggests also a contribution of metamorphic and recycled sedimentary rocks.
- Four divisions or chemofacies (M1, M2, M3 and M4) are represented in the column of the Mirador Formation. These were determined by both element abundance curve and a cluster constrained technique. The most distinct chemofacies is the uppermost, M4, whose chemical signature is very different than those of M1, M2 and M3.
- Differences between chemofacies are governed by changes in the marine influence on the environment, (transition M1–M2), and changes in provenance or relative source rock supply, together with a more mature lithology, suggesting a different deposition condition, probably as result of an interruption in the sedimentary record (transition M3–M4). For instance, the Mirador Formation exhibits changes from bottom to top in some chemical features, which were clearly determined through integrated chemostratigraphic analysis.

**Acknowledgments**—This research was funded by the *Consejo de Desarrollo Científico y Humanístico de la UCV*, through the project CDCH-03.32.4412/1999, and by the CONICIT, through the project No. 97003547. Grateful appreciation is extended to P. Fralick, E. De Carlo, and a third reviewer, who provided helpful comments on the manuscript.

## References


Asiedu, D., Suzuki, S., Nogami, K. and Shibata, T. (2000) Geochemistry of Lower Cretaceous sediments, inner zone of southwest Japan: constraints on provenance and tectonic environment. *Geochem. J.* **14**, 155–173.

Banerjee, I. and Goodarzi, F. (1990) Paleoenvironment and sulfur-boron contents of the Mannville (Lower Cretaceous) coals of southern Alberta, Canada. *Sedimentary Geology* **67**, 297–310.

Bellanca, A., Claps, M., Erba, E., Masetti, D., Neri, R., Premoli, I. and Venezia, F. (1996) Orbitally induced limestone/marlstone rhythms in the Albian-Cenomanian Cismon section (Venetian region, northern Italy): sedimentology, calcareous and siliceous plankton distribution, elemental and isotope geochemistry. *Palaeogeogr. Palaeoclimatol. Palaeoecol.* **126**, 227–260.

Berner, A. (1983) Sedimentary pyrite formation: An update. *Geochim. Cosmochim. Acta* **48**, 605–615.

Bhatt, J. (1974) Ti/Al ratio as chemical index of paleoenvironment—a note. *Chem. Geol.* **13**, 75–78.

Borsier, M. (1991) Automated multielement analysis of geological materials-sample decomposition and inductively coupled plasma (ICP-AES) procedures. *Spectrochim. Acta Rev.* **14**, 79–94.

Brasier, M. and Shields, G. (2000) Neoproterozoic Chemostratigraphy and correlation of the Port Askaig glaciation, Dalradian Supergroup of Scotland. *J. Geol. Soc. London* **157**, 909–914.

Brondjick, J. (1967) Eocene formations in the southwestern part of the Maracaibo Basin. *Asoc. Venez. Geología, Minas y Petróleo, Boletín Informativo* **10**, 35–50.

Colmenares, O. and Terán, L. (1990) Formaciones Mirador y Carbonera: edad y relaciones estratigráficas en el estado Táchira. *Revista Técnica INTEVEP* **10**, 209–212 (in Spanish).

Crespo, S. Sliter, W. and Jarvis, I. (1999) Integrated foraminiferal biostratigraphy and Chemostratigraphy of the Querecual Formation (Cretaceous) Eastern Venezuela. *J. Foraminiferal Research* **29**, 487–499.

Crowley, S., Warwick, P., Ruppert, L. and Pontolillo, J. (1995) The origin and distribution of HAP elements in relation to maceral composition of the A1 lignite bed (Paleocene, Calvert Bluff Formation, Wilcox Group), Calvert Mine Area, East-Central Texas. USGS Open-File Report 95-595, 1–10.

Cullers, R. (2000) The geochemistry of shales, siltstones and sandstones of Pennsylvanian-Permian age, Colorado, USA: implications for provenance and metamorphic studies. *Lithos* **51**, 181–203.

Cullers, R., Basu, A. and Suttner, J. (1988) Geochemical signature of provenance in sand-size material in soil and stream sediments near the Tobacco Root Batholith, Montana, USA. *Chem. Geol.* **70**, 335–348.

Dalrymple, R., Zaitlin, B. and Boyd, R. (1992) Estuarine facies models: conceptual basis and stratigraphic implications. *J. Sedim. Petrology* **62**, 1130–1146.

Das, N. (1997) Chemostratigraphy of sedimentary sequences: A review of de state of the art. *J. Geol. Soc. India* **49**, 621–628.

Dayong, J., Weicheng, H. and Shunliang, B. (1999) Relationship between Milankovitch eccentricity cyclicity and chemo-cycles from the upper Givetian (Devonian) in Guangxi, South China. *Chinese Science Bulletin* **44**, 1697–170.

Dinelli, E., Lucchini, F., Mordenti, A. and Paganelli, L. (1999) Geochemistry of Oligocene-Miocene sandstones of the northern Apenines (Italy) and evolution of chemical features in relation to provenance changes. *Sedimentary Geology* **127**, 193–207.

Dixon, W. and Kronmal, R. (1965) The choice of origin and scale for graph. *J. Association of Comp. Mach.* **12**, 259–261.

Ehrengerg, S., Svånå, T., Paterson, B. and Mearns, E. (2000) Neodymium isotopic profiling of carbonate platform strata: correlation between siliciclastic provenance signature and sequence stratigraphy. *Sedimentary Geology* **131**, 87–95.

Fralick, P. and Kronberg, B. (1997) Geochemical discrimination of clastic sedimentary rock sources. *Sedimentary Geology* **113**, 111–124.

Gill, D., Shomrony, A. and Fligelman, H. (1993) Numerical zonation of Log suites and Log facies recognition by multivariate clustering. *AAPG Bull.* **77**, 1781–1791.

González de Juana, C., Iturralde, J., and Picard, X. (1980) *Geología de Venezuela y sus cuencas petrolíferas*. Caracas, Ediciones Foninves, 1081 pp. (in Spanish).

Hiscott, R. (1984) Ophiolitic source rocks for Taconic-age flysch: trace element evidence. *Geol. Soc. Am. Bull.* **95**, 1261–1267.

Jarvis, I., Moreton, J. and Gérard, M. (1998) Chemostratigraphy of Madeira Abyssal Plain Miocene-Pleistocene turbidites, site 950. *Proc. Ocean Drilling Program, Scientific Results* **157**, 535–558.

Mason, B. and Moore, C. (1982) *Principles of Geochemistry*. 4th ed., John Willey & Sons. 350 pp.

Nesbitt, H. (1979) Mobility and fractionation of rare earth element during weathering of a granodiorite. *Nature* **279**, 206–210.

Paparoni, G. (1993) Análisis y caracterización de litofacies pertenecientes a parasecuencias de edad Eoceno (ambientes de transición), Formación Mirador de Venezuela Occidental. Deg. Thesis, Univ. Central Venez., 301 pp. (in Spanish).

Parnaud, F., Gou, Y., Pascual, J., Capello, M., Truskowski, I. and Passalacqua, H. (1995) Stratigraphic Synthesis of Western Venezuela, in A. Tankard, Suarez and Welsink. *Petroleum Basins of South America: AAPG Memoir* **62**, 681–698.

Pearce, T., Besly, B., Wray, D. and Wright, D. (1999) Chemostratigraphy: a method to improve interwell correlation in barren sequences—a case study using onshore Duckmantian/Stephanian sequences (West Midlands, U.K.). *Sedimentary Geology* **124**, 197–220.

Piovano, E., Ross, R., Guevara, R., Arribére, M. and Depetris, P. (1999) Geochemical tracers of source rocks in a Cretaceous to Quaternary sedimentary sequence (Eastern Sierras Pampeanas, Argentina). *Journal of South American Earth Sciences* **12**, 489–500.

Reiman, C. and Filmoser, P. (1999) Normal and lognormal data distribution in geochemistry: death of a myth. Consequences for the statistical treatment of geochemical and environmen-

tal data. *Environmental Geology* **39**, 1001–1014.
Reinhardt, L. and Ricken, W. (2000) The stratigraphic and geochemical record of Playa Cycles: monitoring a Pangean monsoon-like system (Triassic, Middle Keuper, S. Germany). *Palaeogeogr. Palaeoclimatol. Palaeoecol.* **161**, 205–227.
Reyment, R. and Hirano, H. (1999) Exploratory multivariate statistical analysis of geochemical data from the Cenomanian-Turonian transition of the Yezo Supergroup, Hokkaido, Japan. *Cretaceous Research* **20**, 539–546.
Stevenson, R., Whittaker, S. and Mountjoy, E. (2000) Geochemical and Nd isotopic evidence for sedimentary-source changes in the Devonian miogeocline of the southern Canadian Cordillera. *Geol. Soc. Am. Bull.* **112**, 531–539.
Totten, M., Hanan, M. and Weaver, B. (2000) Beyond whole-rock geochemistry of shales: The importance of assessing mineralogic controls for revealing tectonic discriminant of multiple sediment sources for the Ouachita Mountain flysch deposits. *Geol. Soc. Am. Bull.* **112**, 1012–1022.
Villamil, T. (1996) Depositional and geochemical cyclicity in the cretaceous fine-grained strate of Colombia. A model for organic matter content. *Ciencia, Tecnología y Futuro* **1**, 5–23.
Wedepohl, K. (1995) The composition of the continental crust. *Geochim. Cosmochim. Acta* **59**, 217–239.
Winchester, J. and Max, M. (1996) Chemostratigraphic correlation, structure and sedimentary environments in the Dalradian of the NW Co. Mayo inlier, NW Ireland. *J. Geol. Soc. London* **153**, 779–801.
Yarincik, K. and Murray, R. (2000) Climatically sensitive eolian and hemipelagic deposition in the Cariaco Basin, Venezuela, over the past 578,000 years: results from Al/Ti and K/Al. *Paleoceanography* **15**, 210–228.